Volume 2 | Number 19 | 21 May 2014 | Pages 3661–3856

Journal of Materials Chemistry C

Materials for optical, magnetic and electronic devices

www.rsc.org/MaterialsC

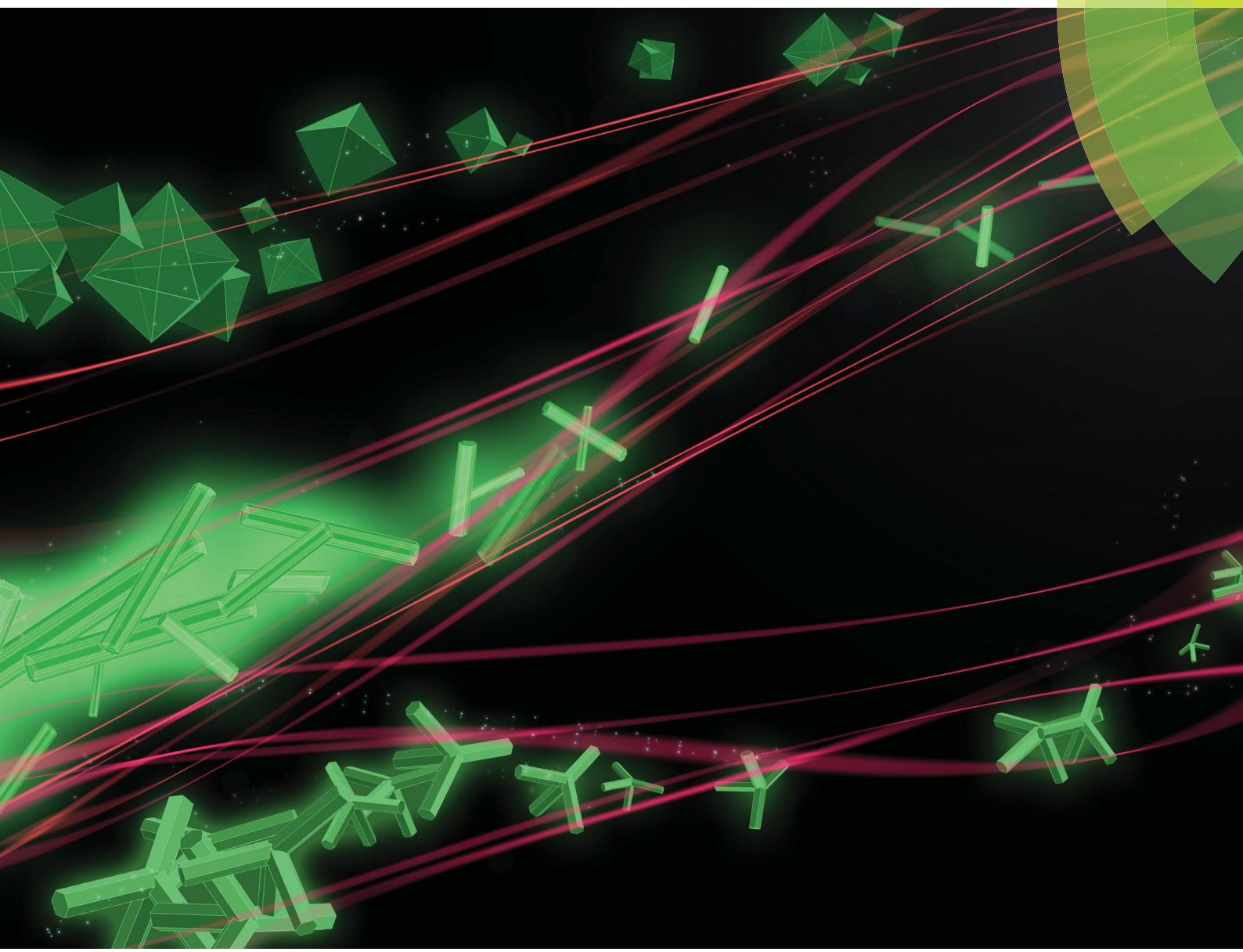

ISSN 2050-7526

ROYAL SOCIETY OF CHEMISTRY

PAPER

Tian Jian Lu, Feng Xu *et al.*

Synthesis of upconversion $NaYF_4$:Yb^{3+},Er^{3+} particles with enhanced luminescent intensity through control of morphology and phase

Journal of Materials Chemistry C

PAPER

View Article Online
View Journal | View Issue

Cite this: J. Mater. Chem. C, 2014, 2, 3671

Synthesis of upconversion $NaYF_4$:Yb^{3+},Er^{3+} particles with enhanced luminescent intensity through control of morphology and phase†

Min Lin,[ab] Ying Zhao,[b] Ming Liu,[c] MuShu Qiu,[ab] YuQing Dong,[b] ZhenFeng Duan,[d] Ying Hui Li,[e] Belinda Pingguan-Murphy,[f] Tian Jian Lu*[b] and Feng Xu*[ab]

Received 22nd January 2014
Accepted 3rd March 2014

DOI: 10.1039/c4tc00129j

www.rsc.org/MaterialsC

Preparation of well-defined $NaYF_4$ crystals with bright upconversion emission remains a major challenge. The complicated chemical reactions as well as the effect of structure, phase and morphology on the emission efficiency require fine tuning of multiple parameters during the growth of $NaYF_4$ crystals. In this study, we successfully synthesized $NaYF_4$:Yb^{3+},Er^{3+} microcrystals with well-controlled morphologies (*e.g.*, sphere and tube) and enhanced luminescent intensity through tuning pH values and ion concentrations in the initial reaction solution. With increasing reaction time, the phase of $NaYF_4$:Yb^{3+},Er^{3+} changes from cubic to hexagonal, while the morphology follows the change from spheres to microtubes and then to microrods. Upon excitation by 980 nm infrared light, hexagonal $NaYF_4$:Yb^{3+},Er^{3+} microtubes show a significant enhancement in green upconversion emission, which is much stronger than that observed in particles with other morphologies. This phase and morphology dependent strong upconversion emission holds great potential for applications in photonic devices and bioanalyses.

1. Introduction

As one of the most important fluorescent materials, lanthanide-doped upconversion materials have attracted increasing interest due to their capability of absorbing and converting lower energy excitations with near-infrared long wavelength to higher energy emissions with short wavelength.[1–6] This unique feature renders these materials with many advantages over organic dyes and quantum dots in biological applications, such as enhanced tissue penetration,[7,8] weak autofluorescence,[9] improved resistance to photobleaching,[10] and lower cytotoxicity.[11] Thus, the lanthanide-doped upconversion materials find widespread applications in biomedicine, such as biological imaging,[3,12] biological sensing/detection,[10,13] development of point-of-care devices and drug delivery.[14–16] For these applications, the enhanced detection signals are highly demanded.[17,18] Therefore, synthesis of lanthanide-doped upconversion materials with superior luminescent properties has become the focus of interest recently.

Rare earth oxides and fluorides have been widely used as host crystals for the synthesis of lanthanide-doped upconversion materials.[19] Among them, β-$NaYF_4$ is one of the most efficient host lattices for generating upconversion emission, thus attracting intensive study in the field of materials science.[20] Rational control over the morphology and phase allows manipulation of micro and nanocrystals with desired properties. Understanding how the luminescent properties change with morphology and phase is of great significance in the design of upconversion materials. Therefore, numerous investigations have been devoted to the synthesis of lanthanide-doped β- and α-$NaYF_4$ micro- and nanocrystals. A hydrothermal route has been successfully employed to synthesize lanthanide-doped β-$NaYF_4$ with various morphologies, such as nanosphere,[21] nanowire,[22] pindle-like microcrystal,[23] microrod,[24] microprism,[25] and octadecahedron.[26] The particle morphologies have been found to have significant effect on the fluorescence properties of lanthanide-doped upconversion materials.[20,24,27] For example, β-$NaLuF_4$:Yb^{3+},Er^{3+} (ref. 28) and β-$NaYbF_4$:Tm^{3+} with microtube shape[29] possess higher fluorescent intensity than those with other morphologies (*e.g.*, cube, rod and prim).

[a]The Key Laboratory of Biomedical Information Engineering, Ministry of Education, School of Life Science and Technology, Xi'an Jiaotong University, Xi'an 710049, P.R. China. E-mail: fengxu@mail.xjtu.edu.cn

[b]Bioinspired Engineering and Biomechanics Center (BEBC), Xi'an Jiaotong University, Xi'an, P.R. China 710049. E-mail: tjlu@mail.xjtu.edu.cn

[c]Electronic Materials Research Laboratory, Key Laboratory of the Ministry of Education & International Center for Dielectric Research, Xi'an Jiaotong University, Xi'an 710049, P.R. China

[d]Center for Sarcoma and Connective Tissue Oncology, Massachusetts General Hospital, Harvard Medical School, MA, USA

[e]State Key Laboratory of Space Medicine Fundamentals and Application, Chinese Astronaut Research and Training Center, Beijing, 100094, China

[f]Department of Biomedical Engineering, Faculty of Engineering, University of Malaya, Kuala Lumpur, 50603, Malaysia

† Electronic supplementary information (ESI) available. See DOI: 10.1039/c4tc00129j

Therefore, it is desirable to synthesize lanthanide-doped $NaYF_4$ with microtube shape to achieve enhanced fluorescent intensity. Although the synthesis of β-$NaYF_4$:Yb^{3+},Er^{3+} microtubes has been achieved by using ethylenediamine tetraacetic acid as an organic surfactant *via* a hydrothermal method[30] and *via* a molten salt method,[31] these two methods either involve an organic substance or require a high reaction temperature (*e.g.*, 350 °C). In addition, the mechanism underlying the morphology evolution and the morphology dependent emission intensity is still not clear. Therefore, there is still an unmet need for developing an environmentally friendly method with mild reaction conditions to synthesize lanthanide-doped upconversion $NaYF_4$ microtubes.

In this study, we have developed a facile and effective hydrothermal method to synthesize $NaYF_4$:Yb^{3+},Er^{3+} microtubes with enhanced luminescent intensity in ultrapure water. Precise control over the particle phase and morphology has been achieved by simply tuning the pH value in the initial solution. The morphology evolution and the growth mechanism of preparing $NaYF_4$:Yb^{3+},Er^{3+} have been studied by controlling the reaction time. The upconversion photoluminescent properties of β-$NaYF_4$:Yb^{3+},Er^{3+} with different morphologies and the possible mechanism that β-$NaYF_4$:Yb^{3+},Er^{3+} microtubes possess the highest luminescent intensity are presented as well.

2. Experimental section

2.1. Preparation

$Y(NO_3)_3\cdot 6H_2O$, $Yb(NO_3)_3\cdot 5H_2O$ and $Er(NO_3)_3\cdot 5H_2O$ were purchased from Alfa Aesar (UK). NaF (with a purity of 99.99%) and HNO_3 were purchased from Tianjin Yong Sheng Fine Chemical Co., Ltd. All of these reagents were used as received without any further purification. We first prepared solutions with three different concentrations of 0.00131, 0.00022 and 0.00011 mol mL^{-1} by dissolving 25 g $Y(NO_3)_3\cdot 6H_2O$, 10 g $Yb(NO_3)_3\cdot 5H_2O$, and 25 g $Er(NO_3)_3\cdot 5H_2O$ into a volumetric flask. The mixture of NaF and $Ln(NO_3)_3$ (Ln^{3+} = Y^{3+}, Yb^{3+}, Er^{3+}) with a molar ratio of 16 : 1 was put into a 50 mL Teflon lined autoclave. The molar ratio of Y : Yb: Er equals 80 : 18 : 2. After 30 min magnetic stirring, 30 mL ultrapure water was added. The pH value was adjusted by dripping a solution of concentrated nitric acid : ultrapure water = 2 : 1 under continuous stirring. The reaction mixture was sealed in a Teflon lined autoclave which was kept in a stainless steel autoclave, and maintained in an oven at 180 °C for 2 h, 8 h and 14 h, respectively. Then, the autoclave was cooled to room temperature naturally, and the product was separated by centrifugation, washed with ultrapure water and ethanol in sequence three times, and then dried in air at 60 °C for 12 h.

2.2. Characterization

The as-prepared samples were characterized by powder X-ray diffraction (XRD) on an XRD-7000 diffractometer with graphite-monochromatized Cu Kα radiation. The morphologies of the samples were obtained by using a field emission scanning electron microscope (SEM), a JSM-6700F. The transmission electron microscopy (TEM) and high-resolution transmission electron microscopy (HRTEM) images were obtained using a JEM 2100 instrument at an accelerating voltage of 200 kV. The upconversion emission spectra were recorded by using a spectrophotometer (QuantaMasterTM40) under external excitation of a 250 mW 980 nm laser diode (RGB Lasersystems). All the measurements were performed at room temperature.

3. Results and discussion

3.1. pH dependent phase and morphology

A. YF_3 octahedron. To determine the crystallinity of the synthesized particles, we performed powder XRD for products prepared at 180 °C for 14 h under various pH conditions such as pH = 1.5, 2.0, and 2.5 (Fig. 1). When the pH value is close to 1.5, the diffraction peaks of the sample can be identified as YF_3 (JCPDS no. 32-1431) showing an orthorhombic phase (Fig. 1a), whereas the reflection peaks of samples from pH near 2.0 and 2.5 are identified as pure hexagonal-phased $NaYF_4$ (β-$NaYF_4$) (Fig. 1b and c), which agree well with the literature values (JCPDS no. 16-0334), except for the sample from pH = 2.0 that has some weak peaks corresponding to cubic-phased $NaYF_4$ (α-$NaYF_4$) (JCPDS no. 06-0342). It is noteworthy that the XRD patterns also indicate that there are differences in the relative intensities of the (100), (110), (101), and (201) peaks for the samples from pH = 2.0 and 2.5, indicating that there may exist different preferential orientation growth.

The morphology of the synthesized particles was characterized using an SEM (Fig. 2a). We observed octahedral microparticles with an average edge length of ~25 μm for samples from pH = 1.5. The higher magnification image of the octahedral microparticles shows sharp edges and a fairly smooth surface (Fig. 2b). The selected area electron diffraction (SAED) pattern of the spot indicates the single crystalline nature of the octahedral microparticles (Fig. 2c). The HRTEM image (Fig. 2d) shows an interplanar distance of 0.198 nm, which can be ascribed to the lattice spacing of (112) planes of YF_3.

B. β-$NaYF_4$:Yb^{3+},Er^{3+} microtubes. At pH = 2.0, the integral morphology of $NaYF_4$:Yb^{3+},Er^{3+} shows a tube shape with outer diameters of 600 nm to 1.2 μm. The wall thickness varies from 170 to 380 nm and the length of the tubes range from 3.8 to 5.8 μm (Fig. 3a). The outer surface of the tubes forms a

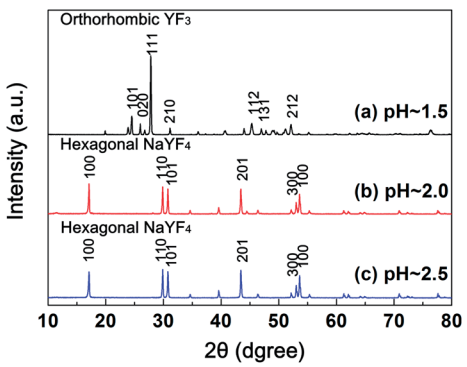

Fig. 1 XRD patterns of the as-prepared products at different pH values: (a) pH = 1.5; (b) pH = 2.0; (c) pH = 2.5.

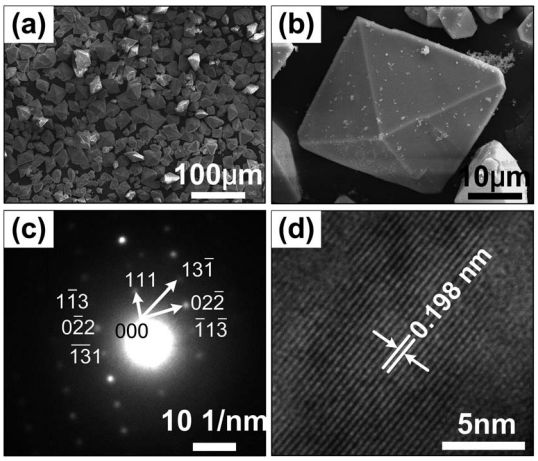

Fig. 2 Low and high-magnification SEM images (a and b), SAED image (c), and HRTEM image (d) of YF_3 obtained at pH = 1.5.

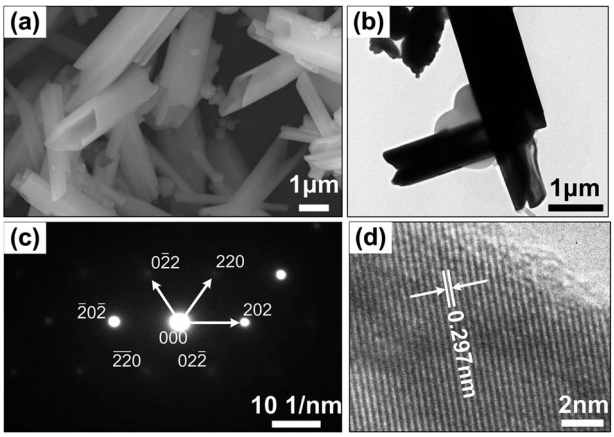

Fig. 3 SEM image (a), TEM image (b), SAED image (c), and HRTEM image (d) of $NaYF_4$:Yb^{3+},Er^{3+}obtained at pH = 2.0.

hexagonal prism and has broken ends. The TEM image also confirms the characteristics of $NaYF_4$:Yb^{3+},Er^{3+} microtubes (Fig. 3b). However, the inner structure cannot be observed clearly in the TEM image due to the large thickness of the tube wall. The corresponding SAED pattern further convinced that the microtubes are single crystalline (Fig. 3c). The obvious lattice fringes in the HRTEM image (Fig. 3d) confirm the high crystallinity of the sample, which agrees well with the XRD results. The determined interplanar distance of 0.297 nm between the adjacent lattice planes (marked by the arrows) is in good agreement with the d_{110} spacing of hexagonal $NaYF_4$:Yb^{3+},Er^{3+}.

C. β-$NaYF_4$:Yb^{3+},Er^{3+} limb-like structure. Once the pH value increased to 2.5, the morphology of the product changed to pseudo-microtube structures with an average length of 2.6 μm and a diameter of 0.85 μm (Fig. 4a). Moreover, there is a small quantity of pseudo-microtubes interconnecting from the centers to form a limb-like structure. Fig. 4b shows the TEM image of $NaYF_4$:Yb^{3+},Er^{3+}, but the entire sample is too large to show its inner structure clearly. The SAED pattern shown in

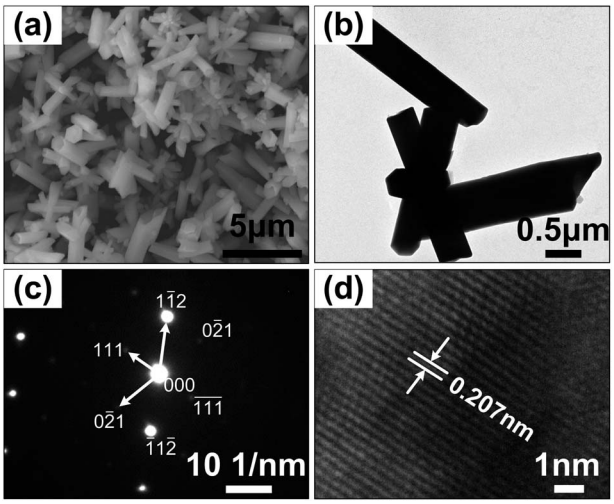

Fig. 4 SEM image (a), TEM image (b), SAED image (c), and HRTEM image (d) of $NaYF_4$:Yb^{3+},Er^{3+}obtained at pH = 2.5.

Fig. 4c displays orderly arranged diffraction spots, indicating their single crystalline nature. The interplanar distance of 0.207 nm could be indexed to the d_{201} spacing of hexagonal $NaYF_4$:Yb^{3+},Er^{3+} (Fig. 4d).

3.2. The growth mechanism of microtubes

To understand the formation and morphological evolution processes of the $NaYF_4$:Yb^{3+},Er^{3+} microtubes, we investigated the time-controlled evolution of $NaYF_4$:Yb^{3+},Er^{3+} microstructures. The XRD pattern and SEM images of the samples prepared with reaction times of 0.5, 8 and 14 h are shown in Fig. 5(a–d). As the samples experience an α → β transformation process, the morphologies evolve during the crystal growth accordingly. Through a set of experiments, the mechanism for the time-dependent morphology evolution is proposed, as shown in Fig. 6. In a very short reaction time (0.5 h), the sample obtained is pure α-$NaYF_4$:Yb^{3+},Er^{3+} (Fig. 5a), which corresponds to spherical-like nanoparticles with a mean diameter of 115 nm (Fig. 5b). The α-$NaYF_4$:Yb^{3+},Er^{3+} seeds have isotropic unit cell structures, inducing an isotropic growth of particles. However, these α-$NaYF_4$:Yb^{3+},Er^{3+} seeds are unstable and phase transformation takes place through a dissolution–nucleation process to form more stable β-$NaYF_4$:Yb^{3+},Er^{3+} (Fig. 5a). A similar formation mechanism has been reported for β-$NaYF_4$:Yb^{3+},Er^{3+} (ref. 32) and β-$NaLuF_4$:Yb^{3+},Er^{3+}.[28] When the reaction time is increased to 8 h, β-$NaYF_4$:Yb^{3+},Er^{3+} microtubes as well as a small amount of α-$NaYF_4$:Yb^{3+},Er^{3+} nanoparticles can be obtained (Fig. 5c). Different from the cubic phase, β-$NaYF_4$:Yb^{3+},Er^{3+} possesses an anisotropic unit cell structure, which leads to an anisotropic growth *via* a dissolution–reconstruction process to form a hexagonal cylinder. Subsequent fast growth on the edges eventually produces β-$NaYF_4$:Yb^{3+},Er^{3+} microtubes with well-defined cross-sections.[28,33–35] Pure β-$NaYF_4$:Yb^{3+},Er^{3+} with a microtube morphology can be achieved when the reaction time is increased to 14 h (Fig. 5d). The morphology of these

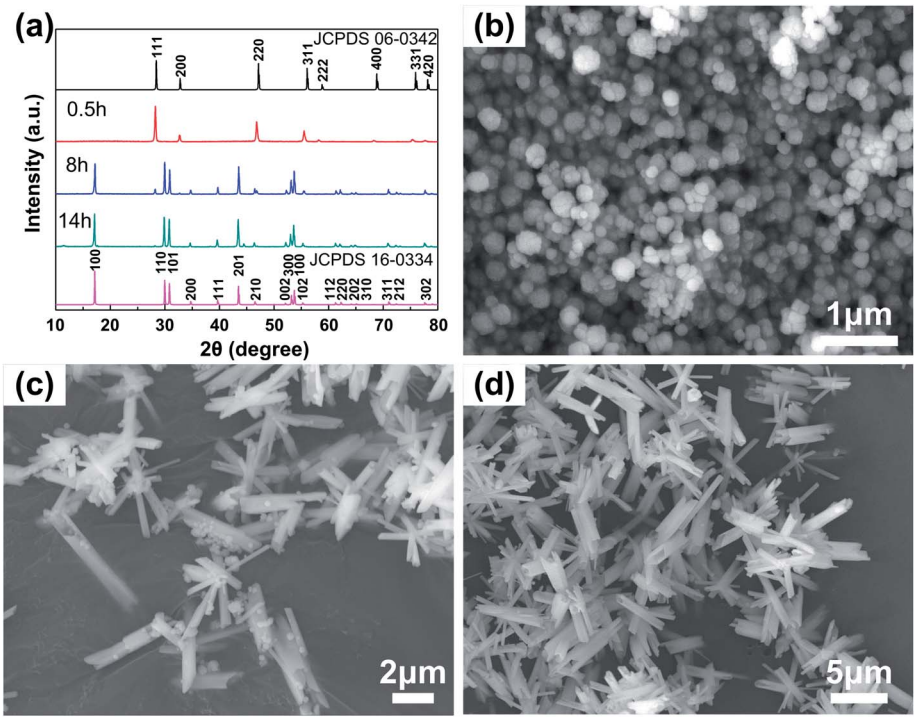

Fig. 5 XRD patterns (a) and SEM images of $NaYF_4$:Yb^{3+},Er^{3+} synthesized with different reaction times of 0.5, 8 and 14 h.

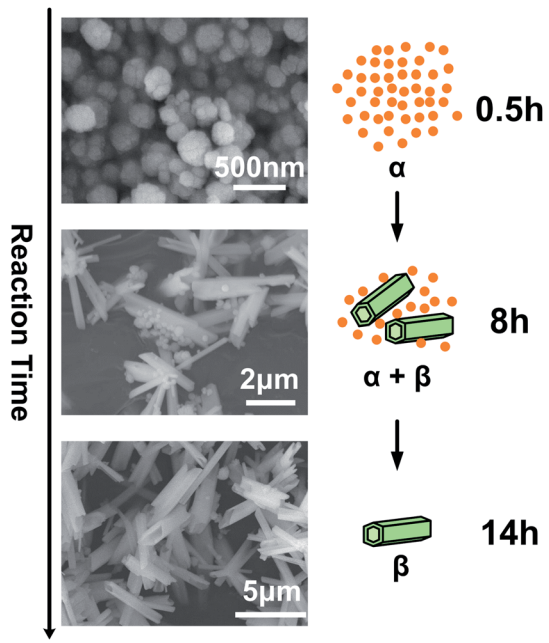

Fig. 6 Schematic diagram of the proposed formation and evolution process of the $NaYF_4$:Yb^{3+},Er^{3+} microtubes crystals.

microtubes does not change much compared to those prepared at 8 h.

3.3. Upconversion luminescent properties

The upconversion luminescence spectrum of the as-prepared products at different pH values (pH = 1.5, 2.0 and 2.5) was acquired under the excitation of a 980 nm laser diode at room temperature. The experimental conditions (*e.g.*, excitation source, excitation intensity and concentration) remain the same for all the samples. Upconversion luminescence emission spectra of YF_3:Yb^{3+},Er^{3+} with octahedral morphology and β-$NaYF_4$:Yb^{3+},Er^{3+} with microtubes and limb-like morphology are shown in Fig. 7. Upconversion emission peaks of green and red

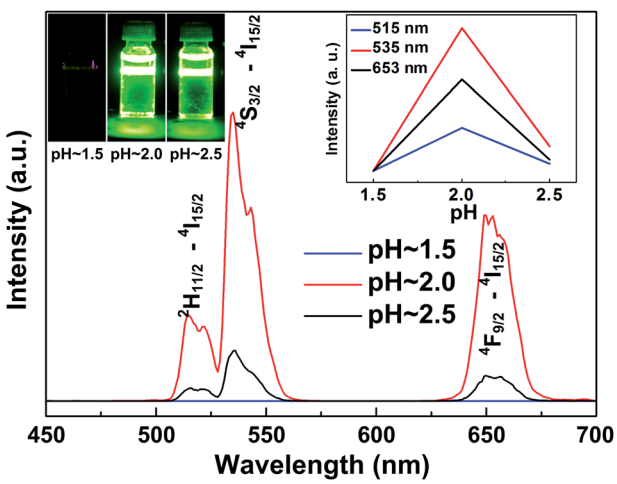

Fig. 7 Upconversion luminescence spectrum of the products prepared at different pH values under excitation by a 980 nm laser: (a) pH = 1.5; (b) pH = 2.0; (c) pH = 2.5. The inset shows the photograph of the samples prepared at different pH values under 980 nm laser excitation (left) and the variation of the green and red upconversion luminescence at different pH values (right). The laser power for excitation was fixed at 250 mW.

centered at 515/535 and 653 nm were observed, which can be assigned to the $^2H_{11/2}/^4S_{3/2} \rightarrow {}^4I_{15/2}$ and $^4F_{9/2} \rightarrow {}^4I_{15/2}$ transitions of Er^{3+} ions, respectively.[30]

Based on the energy matching conditions, possible upconversion mechanisms for Yb^{3+}/Er^{3+} co-doped $NaYF_4$ are discussed on the basis of the simplified energy level diagram as shown in Fig. 8. In the Yb^{3+}/Er^{3+} co-doped system, the pumping light with a wavelength of 980 nm matches the $^2F_{7/2} \rightarrow {}^2F_{5/2}$ transition within the Yb^{3+} ion. After excitation, $^2F_{5/2}$ (Yb^{3+}) transfers energy to the Er^{3+} ion by populating the $^4I_{11/2}$ (Er^{3+}) level. Further excitation from $^4I_{11/2}$ (Er^{3+}) to $^4F_{7/2}$ (Er^{3+}) occurs after energy transfer from the Yb^{3+} ion from a second photon absorption. Transition from $^4F_{7/2}$ (Er^{3+}) to $^2H_{11/2}$ (Er^{3+}) and $^4S_{3/2}$ (Er^{3+}) occurs by a non-radiative energy decay process. Green emission at around 515 and 535 nm results separately from the transitions from $^2H_{11/2}$ (Er^{3+}) and $^4S_{3/2}$ (Er^{3+}) to the ground state $^4I_{15/2}$ (Er^{3+}). Red emission around 653 nm could be attributed to the transition between $^4F_{9/2}$ (Er^{3+}) and $^4I_{15/2}$ (Er^{3+}). The left inset in Fig. 7 shows a photographic image of samples prepared at different pH values. From the images, the green upconversion luminescence can be visually observed by the naked eye. The right inset of Fig. 7 presents the variation of emission intensities as a function of the pH value in the samples. It is clear from the inset that the intensities change obviously with the pH value.

It should be noted that, in all the three samples, the upconversion spectra are similar in shape, and the emission bands differ only in the intensity. The microtubes exhibit the strongest emission intensity, while the octahedral microparticles show a very weak emission intensity, and the relative intensity of the former is about 3 orders of magnitude higher than that of the latter. The difference between upconversion luminescent intensities could be attributed to the combined roles of the phase, morphology and particle size.[24] Based on the XRD patterns of the as-prepared products at different pH values (Fig. 1), β-$NaYF_4$ is a more efficient host lattice than YF_3, so samples prepared at pH = 2.0 and 2.5 have a higher intensity than pH = 1.5. Although the samples prepared at pH = 2.0 (microtube) and 2.5 (limb-like structure) have the same β-$NaYF_4$ phase, the relative intensity of microtubes is almost 6 times as high as that of the limb-like structure. This phenomenon may be caused by the different particle sizes and morphologies. The microtube sample has a larger size as we discussed previously. With increasing crystal size, the Er^{3+} ion concentration on the crystal surface reduces significantly resulting in lower surface defects and stronger emission.[24] Moreover, microtubes have a larger surface area (inner and outer surfaces) than limb-like structures. A larger surface area promotes the absorption efficiency under similar excitation conditions, therefore generating higher luminescent intensity.

It has been demonstrated that ion concentrations have significant influence on the morphology of the as prepared products.[27,36] This will thus affect the luminescent intensity. The influence of the F^-/Ln^{3+} ($Ln^{3+} = Y^{3+}$, Yb^{3+}, and Er^{3+}) ratio on the morphology and phase and the luminescent intensity of the obtained products were therefore discussed and are summarized in the ESI.†

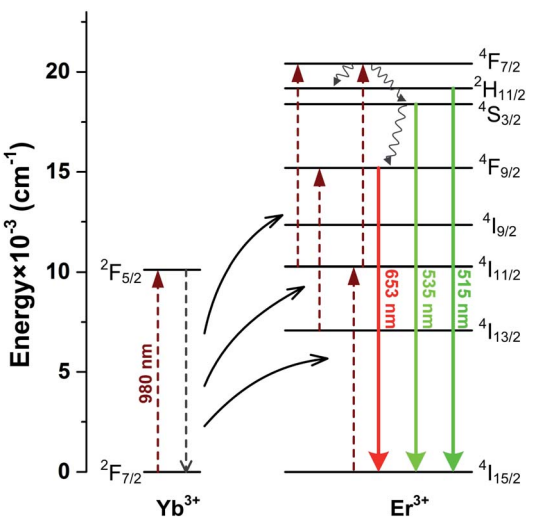

Fig. 8 Schematic illustration of the energy-level diagram of Yb^{3+},Er^{3+} and the mechanism of upconversion emissions.

4. Conclusion

In this paper, we have developed a facile hydrothermal route for synthesis of yttrium fluoride compounds with different morphologies and crystal phases. Without any organic additives, the β-$NaYF_4$:Yb^{3+},Er^{3+} microtubes, β-$NaYF_4$:Yb^{3+},Er^{3+} limb-like structures and YF_3 octahedra can be obtained by simply tuning the pH values in the initial solution. The possible mechanism for the formation of β-$NaYF_4$:Yb^{3+},Er^{3+} microtubes has been studied by performing time-dependent morphology evolution experiments. Moreover, investigation of upconversion spectra of the products under the same measurement conditions reveals that β-$NaYF_4$:Yb^{3+},Er^{3+} microtubes show a considerably stronger luminescent intensity by around 6 times and 3 orders of magnitude than the β-$NaYF_4$:Yb^{3+},Er^{3+} limb-like structure and YF_3:Yb^{3+},Er^{3+} octahedra, respectively. The enhanced luminescent intensity is attributed to the enlarged crystal size and absorption efficiency of β-$NaYF_4$:Yb^{3+},Er^{3+} microtubes. The facile and environmentally friendly method for the synthesis of one-dimensional microtubes will benefit controlled synthesis of other lanthanide-doped rare earth fluoride microtubes with enhanced luminescent intensity for potential applications in bioanalyses and optical devices.

Acknowledgements

This work was financially supported by the National Natural Science Foundation of China (11372243), the National 111 Project of China (B06024), the Major International Joint Research Program of China (11120101002), the Key (Key grant) Project of Chinese Ministry of Education (313045), the South Wisdom Valley Innovative Research Team Program, International Science & Technology Cooperation Program of China (2013DFG02930), National Instrumentation Program (2013YQ190467), and the Fundamental Research Funds for the

Central Universities (2012jdhz46). B.P-M. received funding from the Ministry of Higher Education (MOHE), Government of Malaysia, under the high impact research grant (UM.C/HIR/MOHE/ENG/44). FX was also partially supported by the China Young 1000-Talent Program and Program for New Century Excellent Talents in University (NCET-12-0437). The SEM and TEM work was done at International Center for Dielectric Research (ICDR), Xi'an Jiaotong University, Xi'an, China. The authors also thank Ms. Dai Yan Zhu, Ms. Lu Lu and Mr. Ma Chuan Sheng for their help in using SEM and TEM.

References

1 J. Shen, L. Zhao and G. Han, *Adv. Drug Delivery Rev.*, 2013, **65**, 744–755.
2 Z. Gu, L. Yan, G. Tian, S. Li, Z. Chai and Y. Zhao, *Adv. Mater.*, 2013, **25**, 3758–3779.
3 J. Zhou, Z. Liu and F. Li, *Chem. Soc. Rev.*, 2012, **41**, 1323–1349.
4 D. K. Chatterjee, M. K. Gnanasammandhan and Y. Zhang, *Small*, 2010, **6**, 2781–2795.
5 H. Dong, L.-D. Sun and C.-H. Yan, *Nanoscale*, 2013, **5**, 5703–5714.
6 M. Lin, Y. Zhao, S. Wang, M. Liu, Z. Duan, Y. Chen, F. Li, F. Xu and T. Lu, *Biotechnol. Adv.*, 2012, **30**, 1551–1561.
7 D. K. Chatterjee and Z. Yong, *Nanomedicine*, 2008, **3**, 73–82.
8 D. K. Chatterjee, A. J. Rufaihah and Y. Zhang, *Biomaterials*, 2008, **29**, 937–943.
9 N. M. Idris, Z. Q. Li, L. Ye, E. K. W. Sim, R. Mahendran, P. C. L. Ho and Y. Zhang, *Biomaterials*, 2009, **30**, 5104–5113.
10 F. Zhang, Q. Shi, Y. Zhang, Y. Shi, K. Ding, D. Zhao and G. D. Stucky, *Adv. Mater.*, 2011, **23**, 3775–3779.
11 A. R. Jalil and Y. Zhang, *Biomaterials*, 2008, **29**, 4122–4128.
12 Q. Dou, N. M. Idris and Y. Zhang, *Biomaterials*, 2013, **34**, 1722–1731.
13 Y. Liu, D. Tu, H. Zhu, E. Ma and X. Chen, *Nanoscale*, 2013, **5**, 1369–1384.
14 C. Wang, L. Cheng and Z. Liu, *Biomaterials*, 2011, **32**, 1110–1120.
15 D. Yang, X. Kang, P. Ma, Y. Dai, Z. Hou, Z. Cheng, C. Li and J. Lin, *Biomaterials*, 2013, **34**, 1601–1612.
16 P. L. A. M. Corstjens, L. van Lieshout, M. Zuiderwijk, D. Kornelis, H. J. Tanke, A. M. Deelder and G. J. van Dam, *J. Clin. Microbiol.*, 2008, **46**, 171–176.
17 R. Kattumenu, C. H. Lee, L. Tian, M. E. McConney and S. Singamaneni, *J. Mater. Chem.*, 2011, **21**, 15218–15223.
18 H. Cui, C. Hong, A. Ying, X. Yang and S. Ren, *ACS Nano*, 2013, **7**, 7805–7811.
19 F. Wang and X. G. Liu, *Chem. Soc. Rev.*, 2009, **38**, 976–989.
20 Q. Dou and Y. Zhang, *Langmuir*, 2011, **27**, 13236–13241.
21 Y. Wang, R. Cai and Z. Liu, *CrystEngComm*, 2011, **13**, 1772–1774.
22 D.-K. Ma, S.-M. Huang, Y.-Y. Yu, Y.-F. Xu and Y.-Q. Dong, *J. Phys. Chem. C*, 2009, **113**, 8136–8142.
23 J. Zhuang, X. Yang, J. Fu, C. Liang, M. Wu, J. Wang and Q. Su, *Cryst. Growth Des.*, 2013, **13**, 2292–2297.
24 S. Hao, G. Chen, H. Qiu, C. Xu, R. Fan, X. Meng and C. Yang, *Mater. Chem. Phys.*, 2012, **137**, 97–102.
25 F. Tao, F. Pan, Z. Wang, W. Cai and L. Yao, *CrystEngComm*, 2010, **12**, 4263–4267.
26 L. Gao, X. Ge, Z. Chai, G. Xu, X. Wang and C. Wang, *Nano Res.*, 2009, **2**, 565–574.
27 X. Qu, H. K. Yang, G. Pan, J. W. Chung, B. K. Moon, B. C. Choi and J. H. Jeong, *Inorg. Chem.*, 2011, **50**, 3387–3393.
28 C. Li, Z. Quan, P. Yang, S. Huang, H. Lian and J. Lin, *J. Phys. Chem. C*, 2008, **112**, 13395–13404.
29 S. Zeng, G. Ren, W. Li, C. Xu and Q. Yang, *J. Phys. Chem. C*, 2010, **114**, 10750–10754.
30 J. L. Zhuang, J. F. Liang, H. H. Y. Sung, X. F. Yang, M. M. Wu, I. D. Williams, S. F. Feng and Q. Su, *Inorg. Chem.*, 2007, **46**, 5404–5410.
31 X. Zhang, P. Yang, C. Li, D. Wang, J. Xu, S. Gai and J. Lin, *Chem. Commun.*, 2011, **47**, 12143–12145.
32 Y. Chen, W. He, H. Wang, X. Hao, Y. Jiao, J. Lu and S.-e. Yang, *J. Lumin.*, 2012, **132**, 2404–2408.
33 X. Zhang, P. Yang, C. Li, D. Wang, J. Xu, S. Gai and J. Lin, *Chem. Commun.*, 2011, **47**, 12143–12145.
34 N. Niu, P. P. Yang, F. He, X. Zhang, S. L. Gai, C. X. Li and J. Lin, *J. Mater. Chem.*, 2012, **22**, 10889–10899.
35 C. Li, Z. Quan, P. Yang, J. Yang, H. Lian and J. Lin, *J. Mater. Chem.*, 2008, **18**, 1353–1361.
36 X. Qu, G. Pan, H. K. Yang, Y. Chen, J. W. Chung, B. K. Moon, B. C. Choi and J. H. Jeong, *Opt. Mater.*, 2012, **34**, 1007–1012.

